Understanding disease suppressive soils: molecular and chemical identification of microorganisms and mechanisms involved in soil suppressiveness to Fusarium culmorum of wheat

Ossowicki, A.S.

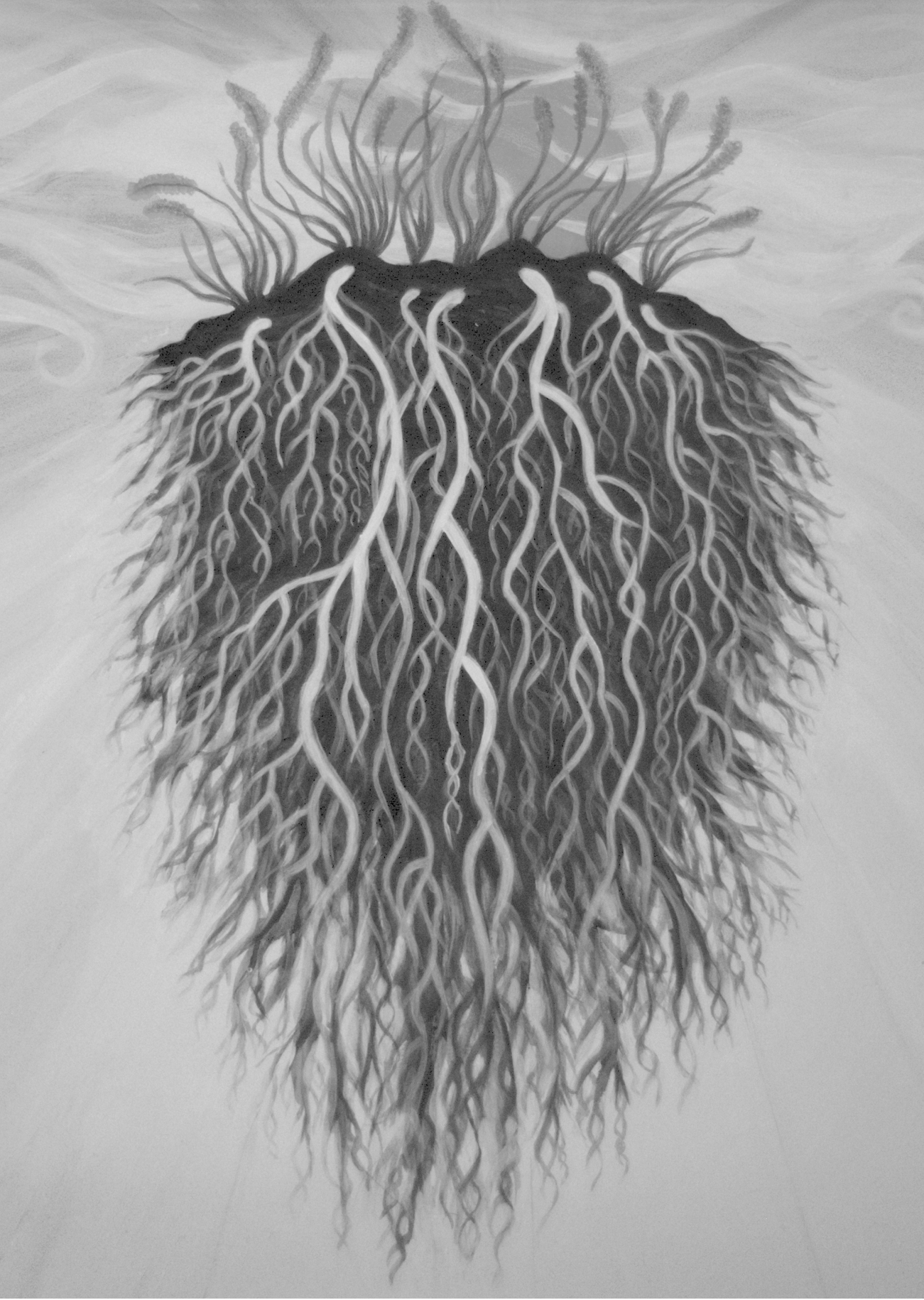

Chapter 4

Deciphering the microbiome of disease suppressive soils by dilution-to-extinction

Adam Ossowicki[1]*, Vittorio Tracanna[2]*, Somayah S. Elsayed[3], Elio G. W. M. Schijlen[4], Mirna Baak[5], Walter Pirovano[5], Gilles P. van Wezel[1,3], Jos M. Raaijmakers[1,3], Marnix H. Medema[2], Paolina Garbeva[1]

1. Microbial Ecology, Netherlands Institute of Ecology (NIOO-KNAW), Wageningen, The Netherlands
2. Bioinformatics Group, Wageningen University and Research, Wageningen, The Netherlands
3. Microbial Biotechnology, Leiden Institute of Biology, Leiden, The Netherlands
4. Bioscience, Wageningen University and Research, Wageningen, The Netherlands
5. BaseClear, Leiden, The Netherlands
*: contributed equally to this work

Abstract

In disease-suppressive soils, root-associated microbiomes provide plant protection against infections by specific soil-borne plant pathogens. Previously, we screened a large number of soils for suppressiveness to *Fusarium culmorum* of wheat and revealed that soil S11 showed a consistent and high level of suppressiveness that was associated with the rhizosphere microbiome. In this study, we used a dilution-to-extinction approach to investigate the underlying mechanisms of microbiome-mediated disease suppressiveness to *F. culmorum*. Our results show that disease suppressiveness can be transferred to a sterile soil by introducing the microbiome extracted from the rhizosphere of wheat grown in suppressive soil S11. Introducing different dilutions of this S11 rhizosphere microbiome into the sterile soil revealed a nonlinear relationship between the dilution factor and the level of disease suppressiveness. At low microbiome dilution, disease was significantly suppressed relative to the untreated control, but the suppressive effect was lost at higher dilutions (100X and higher). Shotgun metagenomic sequencing and reconstruction of 96 metagenome assembled genomes from the rhizosphere microbiota of the different dilutions revealed changes in microbiome composition and functions. We observed a reduction in microbial diversity along the dilution trajectory with an increase in the relative abundance of the Proteobacteria and Bdellovibrionota, and a decrease in the relative abundances of Streptomycetales, Acidobacteria and Verrucomicrobiota. Analysis of the occurrences of KEGG orthologs showed enrichment for 143 orthologs in the suppressive conditions and included terms associated with iron uptake, chitinases and components of the type 6 secretion system. Nine metagenome-assembled genomes were associated with the diminished suppressive phenotype, including a high-quality genome from the bacterial genus *Labilithrix* that contains multiple novel biosynthetic gene clusters. Collectively, this study exemplifies the high added value of dilution-to-extinction to deconstruct a naturally occurring microbiome-associated plant phenotype, i.e., disease suppressiveness. Deciphering the mechanisms and microbial consortia involved in suppressive soils is highly instrumental for the development of new disease management strategies for sustainable agriculture.

Introduction

The thin layer of soil surrounding and influenced by plant roots - the rhizosphere – is populated by diverse microbial communities recruited from the soil microbiome by root exudates (Berg and Smalla, 2009; Morella et al., 2020). Rhizosphere microbes often confer beneficial functions to plants, such as nutrient acquisition, production of phytohormones and protection against biotic and abiotic stresses (Cordovez et al., 2019). Hence, changes in the composition of the rhizosphere microbiome can positively or negatively affect plant

growth and health. For ages, people have recognized that some soils are better for cultivation of particular crops, but only in the last decades we started to understand how microbes present in a soil contribute to better yields and protection from diseases. In so-called disease suppressive soils, the level of disease is low to absent, despite the presence of a virulent pathogen and a susceptible host plant (Raaijmakers and Mazzola, 2011). For most disease-suppressive soils, the protection provided to the plant is mediated by activities of specific members of the soil and rhizosphere microbiota (for reviews see:(Gomes Exposito et al., 2017; Schlatter et al., 2017b; Weller et al., 2002a)). Because of the complex diversity and dynamics of the rhizosphere microbiota (Wagg et al., 2014), unravelling the mechanisms by which specific microbial consortia provide protection against diseases is a challenge. Here we integrated dilution-to-extinction (DTE) and metagenomics to disentangle the microbial traits associated with suppressiveness of soils to *Fusarium* root disease of wheat. DTE is a controlled perturbation method leading to a simplified derivative of the initial microbiome and has been used for manipulation of microbiomes of the gut (Kenters et al., 2011; Lagier et al., 2015) and water (Stingl et al., 2008; Yu et al., 2019) to study rare taxa and ecological succession. Manipulation of microbiome structure and diversity by DTE has also successfully been used in several studies of soil microbiomes in the context of the utilization of carbon sources (Garland and Lehman, 1999), fungistasis (Hol et al., 2015), chitin and cellulose degradation (Peter et al., 2011), antibiotic resistance (Chen et al., 2019, 2017) and general functional potential (Yan et al., 2017). A study by Chen et al. (2020) demonstrated, using a DTE approach, the impact of the microbial taxonomic diversity on soil functions and a positive correlation between microbial diversity and crop productivity (Chen et al., 2020). Korenblum et al. (2020) recently used a combination of DTE with metatranscriptomics and metabolomics to investigate how bacteria reprogram metabolism and root exudation in tomato (Korenblum et al., 2020). The study by Hol et al. (2015) revealed by DTE that reduced taxonomic diversity leads to a reduced ability of the soil microbiota to inhibit the growth of fungal plant pathogens *in-vitro* (Hol et al., 2015). Here, we integrated DTE with metagenomics to identify, for the first time, microbiome functions associated *in situ* with disease suppressiveness to *F. culmorum.* Identifying microbial consortia and microbial functions involved in suppressive soils can substantially contribute to developing new sustainable solutions for future agriculture with reduced inputs of fertilizers and chemical pesticides.

In our previous studies, we screened 28 soils for suppressiveness to *F. culmorum* of wheat and identified several suppressive soils. Amplicon sequencing showed that these suppressive soils did not share the same taxonomic patterns, but co-occurrence network analysis revealed at least one common uniquely overrepresented bacterial guild dominated by *Acidobacteria* (Ossowicki et al., 2020). In some of the suppressive soils, we also found an

association between suppressiveness and the abundance of biosynthetic gene clusters (BGCs) encoding the production of siderophores based on NRPS functional amplicon sequencing (Tracanna et al., n.d.). For the work presented here, we chose agricultural soil S11 because it showed the highest and most consistent level of disease suppressiveness and an association of suppressiveness with siderophore BGCs. For the experimental work, we inoculated a sterile soil with different dilutions of soil S11 and planted wheat. Then, we challenged the plants with the fungal pathogen and monitored disease severity and microbiome dynamics by in-depth metagenomic sequencing. We hypothesize that dilution of the suppressive rhizosphere microbiome i) diminishes the abundance of specific microbial taxa and biosynthetic gene clusters (BGCs) involved in disease suppressiveness, ii) diminishes microbial diversity and thereby disturbs the interactions within the microbial consortia responsible for disease suppressiveness.

Results and discussion

Impact of rhizosphere microbiome dilution on disease suppressiveness

In a greenhouse pot experiment, we extracted the microbiome of disease-suppressive soil S11 grown for 2 weeks to wheat. When introduced into a sterile sandy soil, the extracted soil microbiome (ESM) conferred significant suppressiveness to *F. culmorum* infections of wheat in two independent bioassays with sixteen biological replicates (Fig.1). Dilution of the ESM reduced the level of disease suppressiveness in a non-linear manner. At low dilutions (10X, 25X and 50X), the disease was significantly suppressed, but the suppressive effect was lost at higher dilutions (100X, 200X and 400X) (Fig.1).

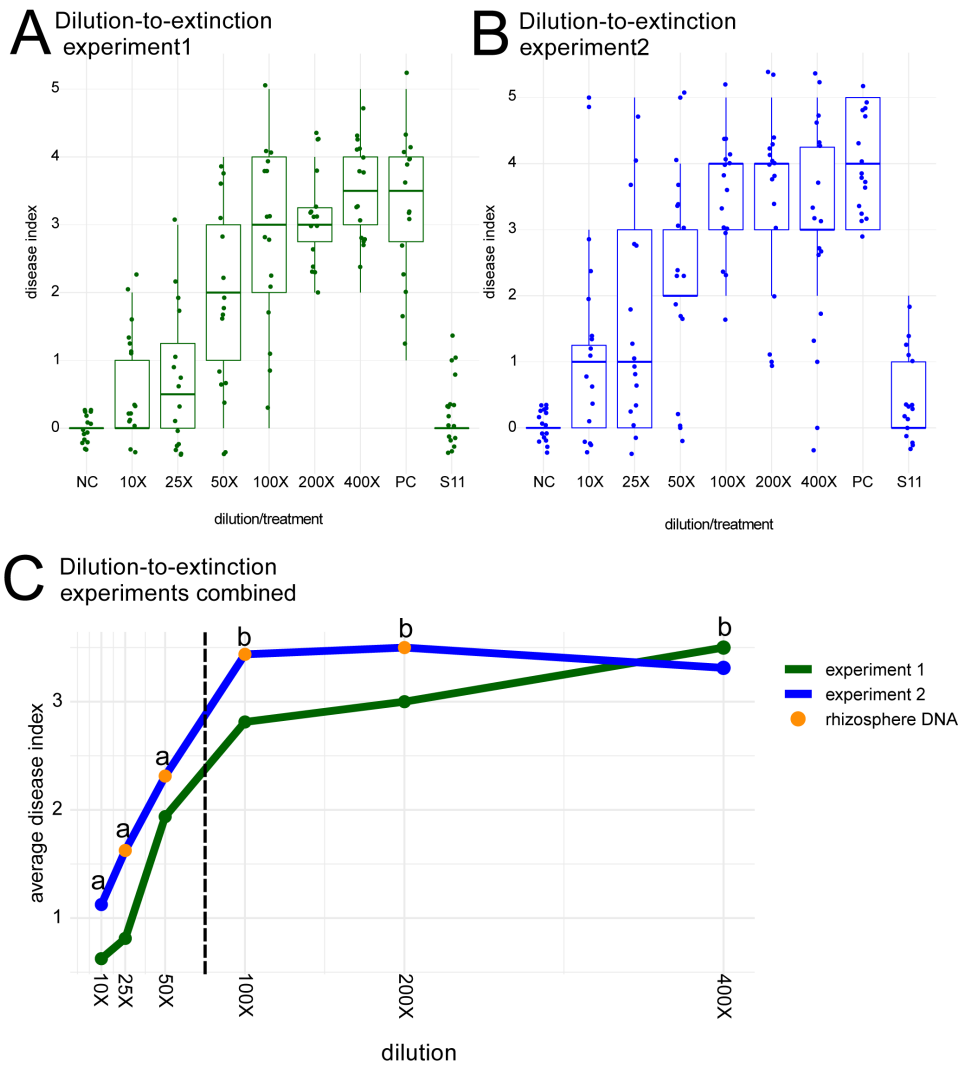

Figure 1. Effects of diluted soil suspensions (10X up to 400X) of disease-suppressive soil S11 on Fusarium culmorum disease severity of wheat plants grown in a sterile soil. Results of two independent experiments (panels A, B) are shown. Disease severity was scored with an index scale ranging from 0 (healthy) to 5 (dead plants). Average disease indices are shown for 16 replicates per treatment. NC is the 'healthy control' where wheat plants are grown in the sterile soil without the pathogen; PC is the 'diseased control' with sterile soil inoculated with the fungal pathogen; S11 is suppressive field soil S11 inoculated with the pathogen. Panel C represents the combined results of the two independent experiments shown in panels A and B. The black dashed line indicates the

transition point in the plant phenotype from suppressive to conducive according to the statistical analyses of the chi-square test; different letters above the data points indicate statistically significant differences. For the metagenome analyses, DNA rhizosphere samples were collected in experiment 2 from the four dilutions indicated by orange dots on the graph.

Dilution-to-extinction is an effective approach to dissect microbiome-associated phenotypes

Following the bioassays, DNA was extracted from the rhizosphere of wheat plants treated with four ESM dilutions that confer phenotypes ranging from disease-suppressive to conducive (non-suppressive). Based on taxonomic classification of the metagenomic reads, the results showed that the rhizosphere microbiomes maintained their overall taxonomic structure at the phylum level over the dilution series (Fig. 2), but the relative abundance of various taxonomic groups significantly changed as a result of the dilution (presented and discussed further below).

The taxonomic distribution was consistent among all five biological replicates of the original extracted ESM and of each of the four dilutions (Fig. S1). According to nonpareil estimation of coverage, the in-depth sequencing efforts for this experiment was able to cover even less abundant and rare members of the rhizosphere microbiota nearly completely (Fig. 3A), providing a basis to deconstruct microbial functions associated with the disease-suppressive plant phenotype while maintaining a similar overall taxonomic composition of the rhizosphere microbiome.

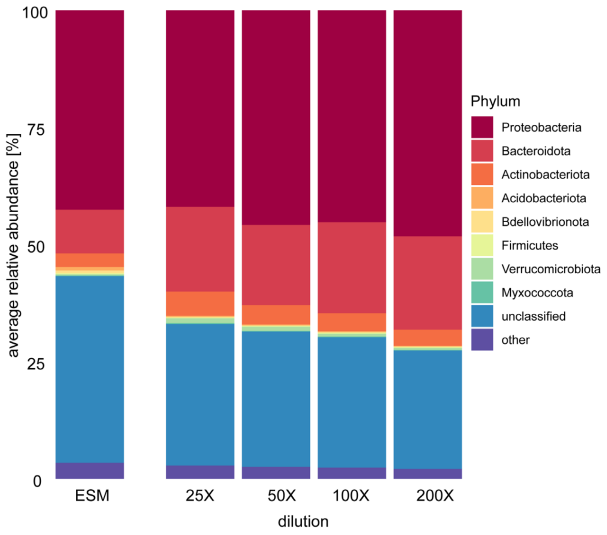

Figure 2. Relative abundance of the bacterial phyla detected in different dilutions of the rhizosphere microbiome of wheat plants grown in Fusarium-suppressive soil S11. ESM represents the extracted soil microbiome, whereas 25X – 200X represent the ESM diluted 25 – 200 times. Taxonomic assignment of the sequence reads was performed using Kraken2 with the GTDB database (Parks et al., 2020; Wood et al., 2019). Averages of 5 replicates are shown.

Changes in microbiome composition and diversity are associated with suppressiveness

Taxonomic annotation at the read level using Kraken2 with the GTDB database (Parks et al., 2020; Wood et al., 2019) showed that the most abundant phyla were Proteobacteria and Bacterioidota. These two phyla together constituted 60 - 68 % of the bacterial community, and their relative share increased at higher ESM dilutions (Fig. 2). Accordingly, the relative abundance of other phyla decreased, except the Bdellovibrionota. *Bdellovibrio* are considered to be potential agents for controlling phytopathogens (Yair et al., 2009; Youdkes et al., 2020), in particular bacterial but not fungal pathogens. The increased relative abundance of Proteobacteria was attributed to the orders of Burkholderiales, Nevskiales, Caulobacterales, Rhizobiales and Sphingomonadales (Fig.4). The relative abundance of Bacterioidota was stable in all the ESM dilutions. Notably, we observed a significant decrease in the relative abundances of taxa previously associated with disease suppressiveness, including the order Streptomycetales (V. Cordovez et al., 2015; Kinkel et al., 2012) and Acidobacteria (Ossowicki et al., 2020; Shen et al., 2015) and Verrucomicrobiota (Chapelle et al., 2016; Navarrete et al., 2015) (Fig.4). In our previous work on comparative taxonomic profiling of disease conducive and disease suppressive soils to *F. culmorum*, including soil S11, co-occurrence network analysis revealed similarities

between the suppressive soils through an overrepresentation of Acidobacteria (Ossowicki et al., 2020). Hence, the results obtained here by metagenomic analysis supports this earlier observation and suggests a potential role of Acidobacteria in suppressiveness to *F. culmorum*. To validate the potential role of Acidobacteria in suppressiveness will require isolation of representative genera and species of this phylum, many of which are still very difficult to culture in laboratory conditions (Costa et al., 2018).

The diversity detected in the twenty rhizosphere metagenomes and in the undiluted ESM was estimated using the database-independent Nonpareil 3 algorithm (Rodriguez-R et al., 2018). The results showed a diversity reduction with increased ESM dilutions (Fig.3B). The major drop in diversity between undiluted ESM and the subsequent dilutions may reflect the selective power of the rhizosphere and the inability of certain groups of microbes to establish and thrive in a sterile soil following inoculation. We noted that the diversity of the rhizosphere metagenomes significantly differed between the lower dilutions (25X and 50X), and the higher dilutions (100X and 200X) (Fig. 3B), which correlates with their contrasting plant phenotypes. In two former studies (Berg et al., 2017; Mallon et al., 2015) it was postulated that the invasion of a pathogen in a biological system, like the rhizosphere, may lead to the extinction of a subset of the resident species, compromising community functioning. It was experimentally shown (from a 'bottom-up' perspective) that reducing the diversity in synthetic bacterial communities made them more susceptible to invading species (Jousset et al., 2011; van Elsas et al., 2012). Our results suggest that the reduced microbial diversity negatively affects disease suppressiveness, supporting the hypothesis that diversity of root-associated microbiomes contributes to plant resilience to biotic stress. In summary, our results showed: i) a reduction in microbial diversity along the ESM dilution trajectory with a concomitant reduction in disease suppressiveness, ii) an increase in the relative abundance of the Proteobacteria and Bdellovibrionota at higher dilutions, and iii)) a decrease in the relative abundances of Streptomycetales, Acidobacteria and Verrucomicrobiota at higher ESM dilutions.

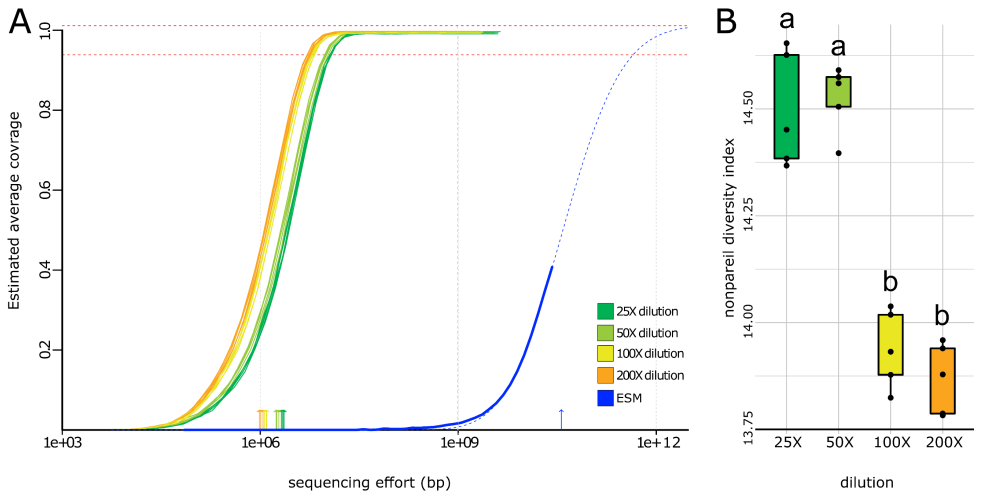

Figure 3. Panel A: estimated sequencing coverage of extracted soil microbiome of suppressive soil S11 (ESM) and rhizosphere microbiomes from different ESM dilutions. ESM coverage for the original extract before inoculation is incomplete (less than 50% of the sequence space is covered) and shows much higher complexity. All the rhizosphere samples cover the genetic diversity of the microbial communities. The curves show a small but consistent separation between low (25X and 50X) and high (100X and 200X) dilutions with lower dilutions displaying higher diversity. Panel B: Effect of diluted suspension of suppressive soil S11 introduced to a sterile soil on genetic diversity of wheat rhizosphere microbiomes expressed as a nonpareil diversity index. The disease symptoms caused by plant pathogen F. culmorum in two lower dilutions 25X and 50X were significantly suppressed compared to higher dilutions 100X and 200X. The significance levels according to ANOVA and Tukey post-hoc test with $p > 0.001$ are indicated by different letters. Full results are presented in Table S1.

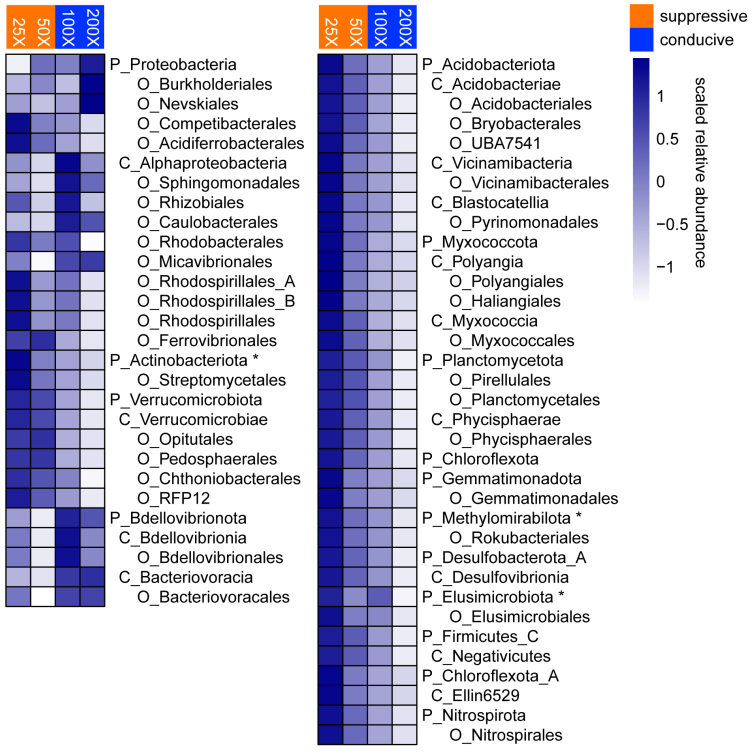

Figure 4. Significant changes in the relative abundance of the rhizosphere bacterial taxa between suppressive soil S11 dilutions exibiting a Fusarium-suppressive (25X and 50X) or a non-suppressive phenotype (100X and 200X). Relative abundance is scaled in rows (z-score), and the name of the taxonomic level is indicated by capital letters: P – Phylum, C – Class, O – Order. The significance of the change in abundance evaluated according to DESeq2 analysis with an adjusted p value < 0,05. The change in relative abundance of taxa marked with an asterisk is not statistically significant, and they are shown to indicate the phylum of lower taxonomic levels. Low abundant taxa (<1%) are not shown on the figure for the clarity of presentation. All the taxa significantly changing abundance are shown in table S2.

Genes associated with iron uptake, chitinase activity and T6SS secretion systems are enriched in disease-suppressive rhizosphere microbiomes

Co-assembly of all rhizosphere metagenome reads (8,214,787,741 reads, 953,849,270,414 Gb) yielded a total of 327,947 contigs above 5 Kb in length with an N50 of 11.908 Kb and total assembly size of 3.638 Gb. The co-assembly strategy was chosen to improve the overall coverage for each organism in the niche, as significant overlap was expected for all samples derived from the same ESM. The KEGG ortholog (KO) functional annotation of diluted

rhizosphere metagenomes reflected the functional potential of the microbial community. As expected in a rhizosphere metagenome, there was a large variety of KEGG orthologous groups (KO groups) with 11,459 unique entries. When investigating a general functional profile of the rhizosphere communities (top and second-level KEGG ortholog categories) across the dilution series showed no statistically significant changes (see supplementary material). To find associations between individual KEGG orthologue groups and the suppressive phenotype, we then separated metagenomic contigs in two categories based on a DESeq2 enrichment test between the lower two dilution points (25X and 50X) versus the two higher dilution points (100X and 200X). Occurrences of KO group annotations for genes of putative suppressiveness-associated contigs were grouped together and tested versus counts in the rest of the assembly. A Fisher's exact test of the occurrences of KEGG orthologs showed enrichment for 143 orthologs after multiple testing correction. Among those, we found terms associated with iron uptake like TonB [ko:K03832] and bacterioferritin [ko:K03594], chitinases [ko:K01183] and components of the Type VI Secretion System (T6SS) [ko:K11894]. Competition for iron was also identified as a potential mechanism of suppression of *F. culmorum* in our previous amplicon-based analyses of nonribosomal peptide synthetase (NRPS) genes (Tracanna et al., n.d.) and previously also for soils suppressive to Fusarium oxysporum (Lemanceau et al., 2009; Mazurier et al., 2009; Siegel-Hertz et al., 2018a; Tamietti and Alabouvette, 1986). The enrichment of NRPS genes involved in siderophore biosynthesis discovered here with untargeted metagenome analysis corroborates our earlier results and highlights the possible contribution of competition for iron in disease suppressiveness to *F. culmorum*.

Chitinases are enzymes involved in degradation of polymeric chitin and often associated with bacteria-fungi interactions (Lacombe-Harvey et al., 2018; Veliz et al., 2017). Production of chitinases was recognized as a potential control mechanism in a soil suppressive to club-root disease of cabbage (Hjort et al., 2014). Also, in a recent study on suppressiveness to *Rhizoctonia solani*, Carrion at al. found the expression of chitinases significantly upregulated in disease-suppressive consortia of root endophytic bacteria (Carrion et al., 2019). However, the enrichment of chitinases in *F. culmorum* suppressive rhizosphere may be related to saprophytic activity of bacteria as well as direct antagonism against the pathogen. Additional experiments are needed to test and validate those scenarios.

T6SS is used by gram-negative bacteria to deliver effectors such as toxins and other pathogenicity factors (Coulthurst, 2013; Records, 2011). T6SS is known to mediate bacteria-bacteria interaction. Nevertheless, some studies suggested a role of T6SS in antagonistic activity of bacteria against fungi (Monjarás Feria and Valvano, 2020; Trunk et al., 2018). While we cannot exclude the incidental enrichment of T6SS components with taxonomic

changes in the microbiome this opens the possibility of a direct inhibition of *F. culmorum* by members of the microbial community which are diminished across dilutions.

Biosynthetic gene clusters and metagenome-assembled genomes associated with suppressiveness

Secondary metabolites are often associated with direct antagonistic activity against fungal pathogens, which can result in disease suppression (Gomez-Exposito et al., 2017; Kwak and Weller, 2013; Schlatter et al., 2017). Microorganisms produce an incredible diversity of bioactive compounds, the production of which is encoded in biosynthetic gene clusters (BGCs). In this study, we identified 42,170 differentially abundant contigs using the DESeq2 package. AntiSMASH prediction of BGCs within this set of contigs yielded 504 BGCs of various classes (Fig.5). Statistical analysis of the distribution of BGC classes in this set versus the whole metagenome showed the enrichment of BGC classes encoding melanin, aryl polyenes and ladderanes in the lower dilutions (Table S4). Melanins in fungi are mainly associated with virulence and protection against physical and chemical stresses (Cordero and Casadevall, 2017). However, they can also be produced extracellularly by diverse bacterial taxa including Streptomycetes which were already found to decrease in abundance at higher ESM dilutions (Fig.4) (El-Naggar and El-Ewasy, 2017). Accordingly, the melanin clusters found in this group share high similarity to other melanin BGCs found in multiple *Streptomyces* strains. Melanins appear to have a role in root colonization by Streptomycetes (Chewning et al., 2019) and considering the relationship between rhizosphere population density and disease suppression (Johnson, 1994; Raaijmakers and Weller, 1998), melanins may indirectly contribute to the disease-suppressive phenotype by increasing the fitness of key microbes involved in suppression of the pathogen. The enrichment of aryl polyenes and ladderanes is discussed in supplementary material.

Considering that BGC classes are generally broad and functionally heterogeneous, we focused our attention on specific gene clusters for which the abundance strongly correlates with the changes in the suppressive phenotype. Among them, we noted delftibactin, pyoverdine, myxochelin and unknown siderophores, including NRPS containing TonB-dependent siderophore receptor) as well as multiple fragments or analogs of BGCs encoding metabolites with reported antifungal properties such as caniferolides (Pérez-Victoria et al., 2019) and Kutznerides (Dong Zhang et al., 2020). Full antiSMASH results can be accessed online ("AntiSMASH results," 2021). However, given such a large collection of potential targets, which in most cases cannot be associated to previously characterized gene clusters in the MIBiG database, we first prioritized those BGCs present in the metagenome-assembled genomes (MAGs) as it can provide additional genomic and taxonomic context (Fig. 5). Manual curation of individual bins resulted in a collection of 96 MAGs. Then, we analyzed the MAG collection looking for BGCs that become differentially abundant along

the ESM dilution trajectory. This resulted in 9 MAGs that were strongly associated with disease suppressiveness and belonged to the bacterial families Burkholderiaceae, Acidimicrobiaceae, Verrucomicrobiaceae, and Polyangiales (Fig. 5 and Fig. 6). Among the 9 MAGs, the ones assigned to the genera *Labilithrix* (Polyangiales) and *Prosthecobacter* (Verrucomicrobiaceae) belong to taxa that displayed a significant decrease in abundance at higher dilutions (table S2). We then linked the KEGG orthologues enriched genes to the MAGs and found that out of the 9 MAGs, only the *Labilithrix* bin contained genes from the previously discussed categories such as chitinase, siderophores associated genes and core T6SS associated genes (Fig. 8). Additionally, we found multiple copies of the T6SS component FHA (Forkhead-associated domain) that was enriched in the dilutions with a suppressive phenotype within the same *Labilithrix* MAG. One particular multimodular NRPS gene cluster stood out, as it is predicted to encode a peptide with 11 modules, does not have a thioesterase termination domain in the BGC region and lies on a contig edge suggesting that it is a fragment of an even larger BGC (Fig. 7). AntiSMASH clusterblast and knownclusterblast results showed little to no similarity to previously encountered and classified clusters, including those from its closest representative in the NCBI database. *Labilithrix* and closely related bacteria were, so far, never associated with disease suppressiveness but have been recognized as producers of antibacterial, antifungal and antiviral agents (Mulwa et al., 2018; Weissman and Müller, 2009; Yamamoto et al., 2014). Future experiments on this genus should aim at the identification of BGCs expressed on roots of wheat challenged with *F. culmorum* and the expression levels correlating with the disease suppressive phenotype. Additionally, previous studies successfully established synthetic communities from disease suppressive endosphere isolates that were able to reproduce the suppressive phenotype (Carrión et al., 2019). Here, we describe a set of 9 MAGs which constitute suitable candidates for initial leads in this direction.

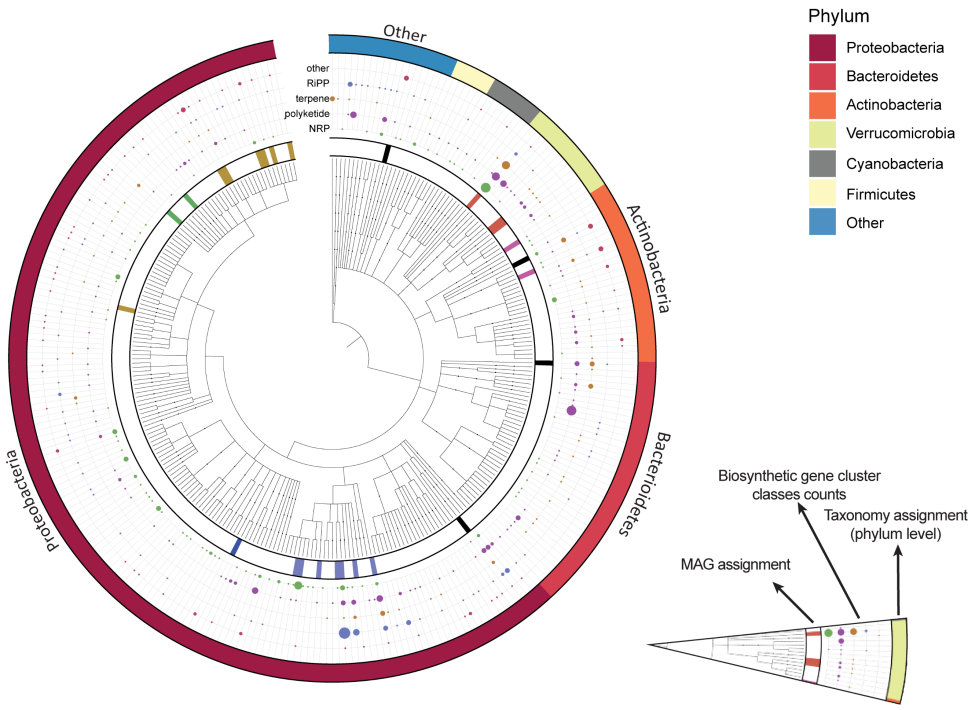

Figure 5. Taxonomical representation of 504 differentially abundant contigs containing biosynthetic gene clusters from the dilution metagenomes. A phylogenetic tree based on their taxonomical annotation is used to order the contigs. In this visualization, contigs assigned to the same taxa are grouped together. The innermost circle (MAG assignment) represents the taxonomic groups containing contigs assigned to a specific metagenome-assembled genome. Contigs assigned to the same MAG are marked with the same color (further description in Fig.7 for a color legend) or with black for MAGs containing only one BGC-harboring contig. For example, the contigs assigned to the L. luteola (Polyangiacee) MAG at approximately 180 degrees are shown in blue both in this inner ring and in Fig 7. Further, the major antiSMASH -predicted BGC classes in the contigs are indicated with dots. The number of predicted BGC is reflected by the size of the dot. Finally, the outer ring represents the contig taxonomical assignment at the phylum level.

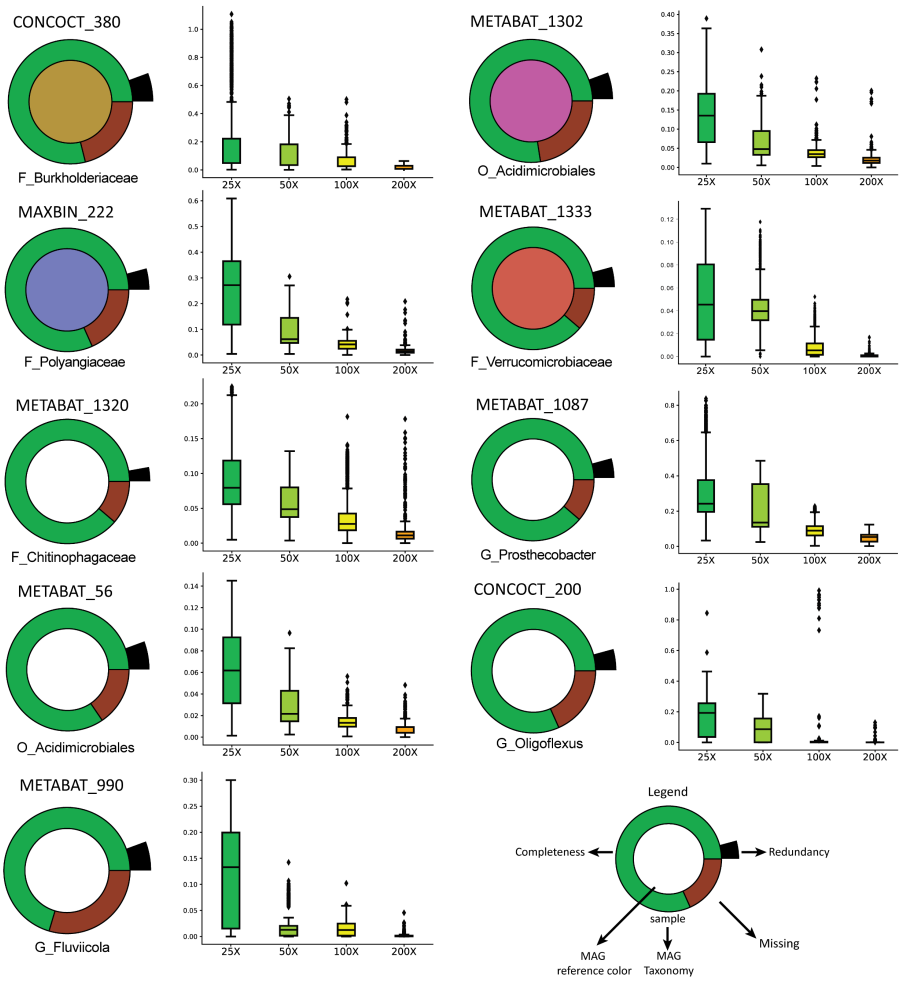

Figure 6. Representation of the MAGs from the metagenome showing significant association with the suppressive phenotype. The MAGs shown here are constituted by 50% or more in length by differentially abundant contigs according to DESeq2 analysis. The ring shows an overview of the MAGs assembly completeness and redundancy. For each MAG, a boxplot shows the abundance of all its contigs across the dilutions. MAG reference colors refer to Fig. 5. The taxonomic levels are inndicated by a capital letters: O – Order,F -family, and G – genus.

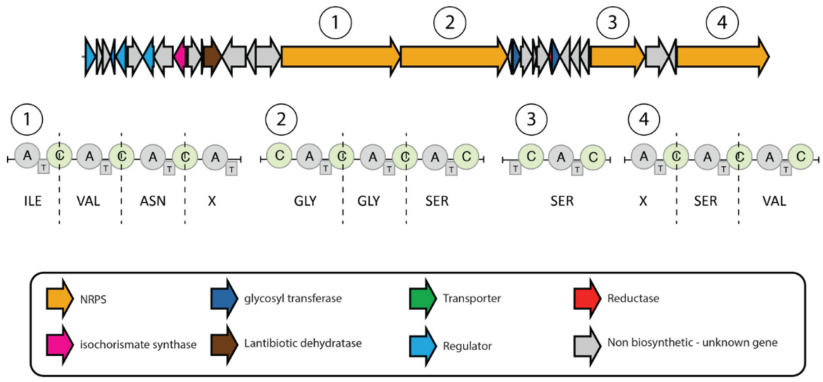

Figure 7. Large NRP gene cluster within Labilithrix MAG with predicted amino acid specificities for each module. The cluster lays on a contig edge and is missing a TE domain and is therefore considered incomplete.

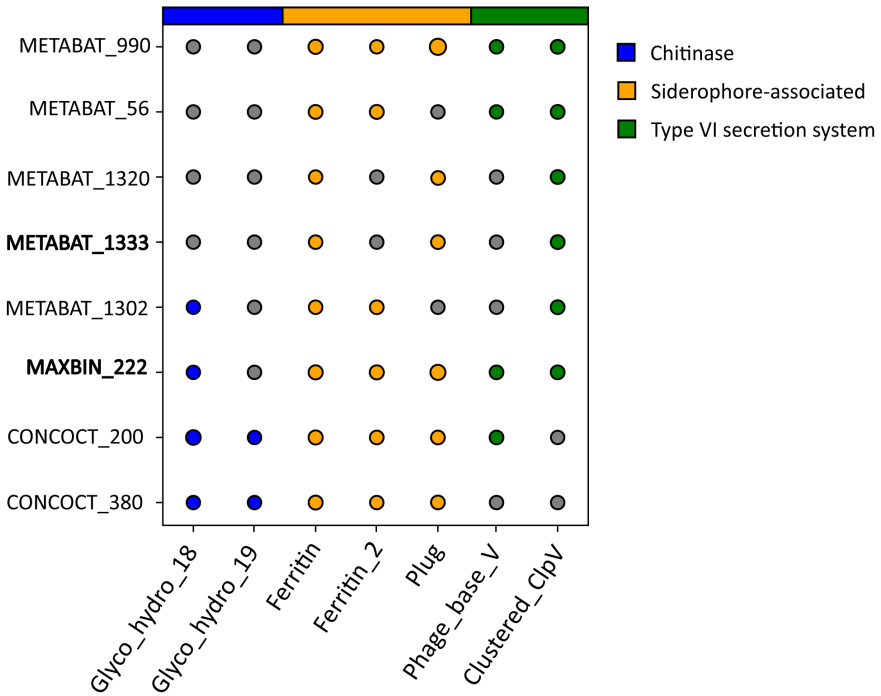

Figure 8. Presence (colored dot) absence (gray dot) patterns of domains contained in KEGG orthologues genes enriched in suppressive dilution points in the MAG collection. Bacterial chitinase families are shown in blue, siderophores associated domains in yellow

and core-representative-components of type VI secretion system in green. Presence of both Phage_base_V and co-occurrence of all 4 ClpV subdomains (AAA, AAA_2, AAA_lid_9 and ClpB_D2-small) on the same contig are considered as minimal requirements for putative presence of type VI secretion system.

Conclusions

We analyzed the microbiome of disease suppressive soil by integrating a dilution-to-extinction approach with shotgun metagenomics. The dilution of the rhizosphere microbial community of the *Fusarium*-suppressive soil led to the decline of the plant protective effect. The dilution effect produced significant changes in the abundance of multiple bacterial taxa and diversity, but these changes could not directly be matched by shifts in the microbiome functional profile. Nevertheless, key BGCs associated with chitin degradation and siderophore biosynthesis were associated with the disease suppressive phenotype. These genes were also detected in the metagenome assembled genomes (MAGs) with yet unknown secondary metabolite production potential. Altogether, this work represents the first example of the dissection of the rhizosphere microbiome of a disease-suppressive soil by using a dilution-to-extinction. This approach could be instrumental in future studies for discovering the mechanisms involved in other soil functions.

Materials and Methods

Soils used in the study

Soil S11 was collected from an agricultural field near Bergen op Zoom, the Netherlands in March 2018. This soil exhibited a high level of disease suppressiveness against *Fusarium culmorum,* which was evaluated in our previous study (Ossowicki et al., 2020). Furthermore, we used a sandy dune soil (BS) collected near Bergharen, the Netherlands (Schulz-Bohm et al., 2015). After collecting soils were air-dried in room temperature, sieved through 4 mm sieve, and stored at 4°C. BS soil was additionally gamma sterilized (Synergy Health Ede B.V., The Netherlands) before use.

Seed preparation and growth conditions

JB Asano wheat seeds (Agrifirm, The Netherlands) were surface sterilized and pre-germinated in order to use in the experiment. Briefly, after surface sterilization with 70% ethanol and 10% bleach, seeds were washed with an excess of sterile water and placed on a wet 1mm paper filter (VWR, the Netherlands). Three-day-old seedlings were transferred to the soil, watered every second day and supplemented weekly with 0,5 Hoagland solution without microelements (0.5 M Ca(NO3)2·4H2O, 1 M KNO3, 1 M KH2PO4, 0.5 M MgSO4·7H2O and 98.6 mM ferric EDTA). Plants were grown in cabinets (MC 1750 VHO-EVD,

Snijders Labs) at 20°C day and night, photoperiod 12 h day/12 h night with 60% relative humidity.

Inoculation and disease suppressiveness evaluation

Soilborne pathogen *F. culmorum* PV (de Boer et al., 1998) was grown on ¼ strength PDA media (Oxoid, The Netherlands) for 2 weeks at 20°C in order to use in the experiment. Where indicated, the pathogen was introduced to the soil before seedling transfer as 6mm mycelium plugs (1 per 10cc of soil). After the experiment wheat plants were gently removed from the soil and cleaned. The disease symptoms on the roots were assessed according at a scale from 0- healthy to 5-severely diseased, like we described before (Ossowicki et al., 2020). Statistical differences in disease symptoms between treatments and control were assessed using the chi-square test, with an alpha cut-off of $p<0.05$.

Microbiome extraction

Wheat plants were grown in four 130 cc pots filled with S11 for two weeks. In order to perform a liquid extraction of the microbiome from the suppressive soil S11, all the glassware, materials and buffer were autoclaved. Plants were gently removed from the pots and the soil with the whole root system was transferred to a glass bottle with 10 volumes of phosphate buffer (10 mM KH_2PO_4, pH=6.5) and 5g of sterile glass beads. These bottles were shaken using an orbital shaker for 1 h at 180 rpm, sonicated for 15 min and shaken again for 1h to detach microorganisms from soil particles. Afterwards, all the extracts were merged in one beaker and sieved through a metal sieve to separate bigger soil particles and roots. Subsequently, extract was briefly centrifuged (1000 x g, 1 min) and the supernatant was filtered again using a Buchner funnel through a filter paper (VWR Grade 415 Filter Paper, VWR the Netherlands). The extract obtained this way was considered a 10X diluted Extracted Soil Microbiome (ESM) because the soil was extracted with 10 volumes of the buffer. In parallel, as a control, the same procedure was applied with the sterile soil BS with a sterile vermiculite (Agra-vermiculite, The Netherlands) in a 1 to 1 volume ration. This way a BS control extract was obtained.

Dilution to extinction - introduction to a sterile soil

In order to optimize the magnitude of the dilution we performed preliminary experiments (data not shown) investigating first, if dilution affects soil disease suppressiveness to *F. culmorum* (the phenotype), and second, at which dilution point the change in phenotype from suppressive to conducive occurs. After the preliminary experiments we chose the dilution steps in such a way that the phenotype tipping point occurs centrally. Compared to the dilution steps used in other studies (Chen et al., 2020; Hol et al., 2015; Korenblum et al., 2020; Yan et al., 2015), we applied a relatively small dilution magnitude. Nevertheless, in

the experimental system we present in this work, these small dilution steps allow us to observe a gradual change of the phenotype.

The 10X dilution of the ESM was serially diluted with phosphate buffer to 25X, 50X, 100X, 200X and 400X and stored at 4°C. The dilution range was determined in a preliminary experiment (data not shown). Plastic, 100 cc pots were filled with the sterile soil BS mixed with sterile vermiculite in a volume ratio of 1 to 1 and with mycelium plugs of *F. culmorum* or sterile ¼ PDA plugs (mock inoculation) according to the treatment. Distinct dilutions of the ESM and the BS control extract were added to pots, 20 ml per day for seven days, before wheat seedlings were introduced. Plants were grown for 3 weeks before the disease assessment and a rhizosphere DNA isolation.

Dilution to extinction - experimental setup

All the dilution treatments and controls consisted sixteen biological replicates, plants were grown in a randomized order to minimize spatial bias. A negative control and a positive control, with and without the pathogen, respectively, were used to control for the infectiousness of the pathogen and the effect of the sterile soil, buffer, and the extraction procedure. The control S11 contained natural suppressive soil S11 with the pathogen introduced to control for the soil disease suppressiveness of the soil that was used for microbiome extraction.

The experiment was performed twice, and the rhizosphere samples used for the DNA extraction were collected in the second experiment from randomly selected replicates.

Rhizosphere DNA extraction

Five out of sixteen replicates were randomly selected for a rhizosphere DNA extraction before the disease assessment. Plants were gently removed from the pots and the soil loosely adhering to the roots was removed by shaking. The whole root system was placed in a 50 ml falcon tube with 25 ml of sterile MQ grade water. The tubes were vortexed, sonicated, and vortexed again, each step for 1 min. Afterwards, the roots were removed with sterile forceps and disease symptoms were assessed on them. The water with extracted rhizosphere was briefly spined down (1000 x g, 1 min) and carefully decanted to a new 50 ml falcon tube. The decanted liquid was frozen at -20 °C and freeze dried overnight (Free zone 12, Labconco the USA). This resulted in forming a white powder in the tube which was collected and extracted using a DNeasy PowerSoil Kit (QIAGEN, the Netherlands) according to the manufacturer's protocol, without applying a bead beating step. Samples were subsequently purified using the DNeasy PowerClean cleanup kit (QIAGEN, the Netherlands).

Data quality control, assembly, mapping and binning

Raw paired sequence reads were quality-checked with (Andrews, 2015) and trimmed using bbduk (Bushnell, n.d.) with a Phred score threshold of 30. Read pairs for which at least one mate was shorter than 150 bp were discarded. Reads for all dilution points were co-assembled in a single assembly using megahit v1.2.9 (Li et al., 2016). Genes were predicted using prodigal v2.6.3 (Hyatt et al., 2010) using the metagenome mode. Reads were mapped back onto the assembly contigs using hisat2 (Kim et al., 2019). BAM files were converted into SAM using samtools v1.7 and rpkm counts were obtained with the mpileup (Li et al., 2009). Binning was performed within anvi'o environment v6.2 (Eren et al., 2015) using DASTOOL (Sieber et al., 2018) refinement of MAXBIN2 v2.2.7 (Wu et al., 2016), CONCOCT v1.1.0 (Qian and Comin, 2019) and METABAT v2.15 (Kang et al., 2019) obtained bins. MAGs with a DASTOOL confidence score >= 0.5 were kept.

Enrichment analysis, biosynthetic gene cluster annotation, reads taxonomy annotation and KEGG functional annotation

Identification of differentially abundant contigs was performed in R using DESeq v1.18.1 (Love et al., 2014, p. 2) looking for enrichment of contigs in the first two dilution points (25X and 50X) versus the higher dilution points (100X and 200X). Contigs with adjusted p-value < 0.05 were considered differentially abundant. Biosynthetic gene clusters were predicted from differentially abundant contigs with a positive fold change using antiSMASH 5.1.2 (Blin et al., 2019) using the prodigal-meta option for gene prediction, --cb-general and --cb-knownclusters for comparison of predicted clusters to antismash-database (Blin et al., 2020) and MIBiG (Kautsar et al., 2020). Quality-trimmed reads were taxonomically annotated using kraken v2.0.8 (Wood et al., 2019) against the GTDB-taxonomy database release 05-RS95 (Parks et al., 2020) KEGG annotation was performed at Baseclear (Leiden, The Netherlands) using the full megahit assembly.

Phylogeny tree construction and annotation

Differentially abundant contigs which had at least one predicted cluster were taxonomically annotated using diamond v 0.9.21 (Buchfink et al., 2015) against the NCBI nr database Oct. 2020 (NCBI Resource Coordinators, 2016). Contigs were assigned to the taxonomical group with the highest cumulative score across the contig. Contigs annotated with the same taxonomy were grouped for tree construction. The list of taxonomic groups was used in NCBI common tree to obtain a tree in PHYLIP format representing the phylogeny relations of the taxonomies present in the differentially abundant contigs with biosynthetic gene clusters shown in Figure 5. Annotation of the tree was done with iTOL (Letunic and Bork, 2019) and is available at https://itol.embl.de/tree/8873156232367181606086331#.

Presence-absence of KEGG orthologs enriched domains in MAGs was determined using hmmsearch v3.1b2 (Mistry et al., 2013) and hmm domains from pfam (El-Gebali et al., 2019) against the different MAGs using trusted cutoffs. Presence of ClpV was determined based on the co-occurrence of all 4 ClpV subdomains (AAA, AAA_2, AAA_lid_9 and ClpB_D2-small) on the same contig. ClpV and Phage_base_V are considered core components of type VI secretion system (Boyer et al., 2009).

Supplementary material

General functional profiles of the rhizosphere microbiomes are resilient to dilution

We grouped KEGG orthologs by their KEGG Orthology hierarchical classification and aggregated their RPKM counts to generate functional profiles for each sample per KO category. Interestingly, no category with a sufficient number of entries was found to be significantly different across the dilutions (Fig. S3), including categories which contain differentially abundant KOs.

From these observations, we deduce that, despite the changes in the taxonomic profiles, the KO functional profiles of the communities are generally stable at the level of these broad categories across dilutions, with no statistical differences (Fig.S3). This may be connected to the strong selective pressure of the environment, which restricts members of the community into a well-defined functional profile. In our experiment, every rhizosphere community occupied highly similar niche; therefore, we can conclude that the general functional profiles could also be highly similar. We can speculate that further dilutions of the ESM inoculum would have a stronger effect on the metabolic profiles, as shown in the work of Yan et al. (Yan et al., 2017). Nevertheless, it would also disturb the community in considerable way and our intention in this experiment was to track the changes in microbial communities related to the change in disease suppressiveness which were shown to be significant between these dilution points. The loss of the suppressive phenotype across the dilutions without significant changes in functional profiles suggests that the origin of this phenomenon is not related to specific community-wide microbiome features but to specific "silver bullets" which cannot be tracked with large scale functional analysis.

Because of the character of KEGG database (Kanehisa et al., 2017) we can only draw conclusions about the general functional profiles of the soil microbial communities. To understand the specialized secondary metabolism of soil microbiomes, which was recognized to be crucial for soil suppressiveness in a number of studies (Gomes Exposito et al., 2017; Kwak and Weller, 2013; Schlatter et al., 2017b), we need to use other approaches. To this end, we decided to expand the functional analysis with prediction and identification of biosynthetic gene clusters (BGC) using antiSMASH pipeline (Blin et al., 2019).

Additional enriched gene cluster classes in suppressive rhizosphere

In addition to melanins, two more BGC product classes were significantly more present in suppressive enriched contigs compared to the rest of the metagenome: aryl polyenes and ladderane. The functional role of aryl polyenes produced by rhizosphere bacteria is so far unknown. This class of antioxidants is similar to carotenoids in structure and biochemical function and likely protect bacteria from reactive oxygen species produced by the plant as a response to infection (Lehmann et al., 2015). The synthesis genes of aryl polyenes are

abundant among Proteobacteria but not in Alphaproteobacteria and Gammaproteobacteria (Schöner et al., 2016). Since Alphaproteobacteria are the main contributors to the increased abundance of whole phylum in high dilutions, it is likely that also the enrichment of the aryl polyene BGCs is related to the abundance of associated taxa. Laddreanes are membrane lipids present in anammoxosomes – intracellular compartments of ammonium-oxidizing bacteria (Hancock and Brown, 2021). Since, these lipids are mostly found in Planctomycetes (Sinninghe Damsté et al., 2005) we can attribute the ladderane BGCs enrichment to the abundance of this group (Fig.4). Ladderanes are predominantly found in marine environments and their role in rhizosphere is unknown. Despite their enrichment in suppressive associated contigs, these biosynthetic gene cluster classes have no known association with antifungal activity nor provide fitness competitive advantage over the pathogen. Therefore, we consider this enrichment incidental to the relative decrease in abundance of the corresponding producing taxonomic groups.

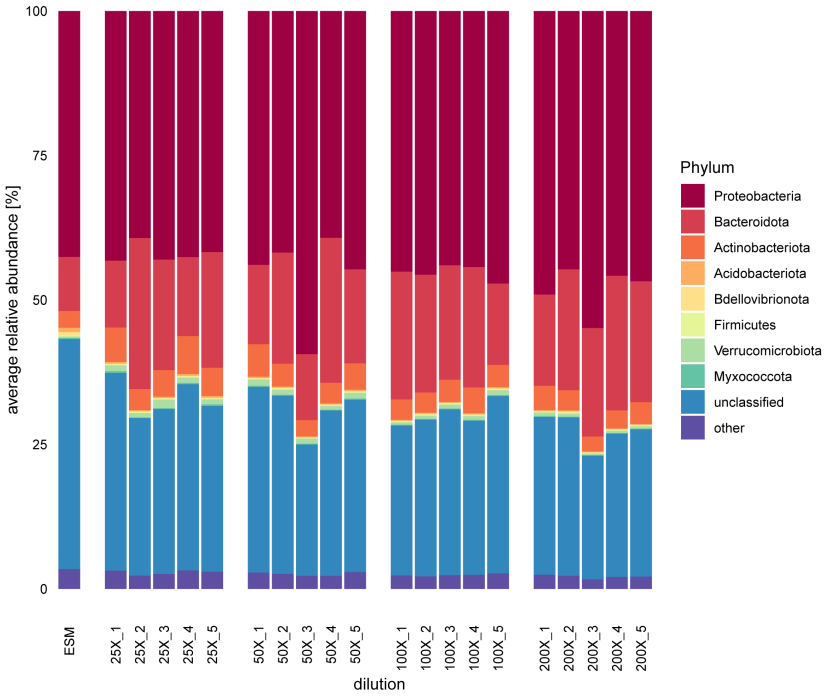

Figure S1. Barplot showing the most abundant phyla in the ESM and rhizosphere across four dilution points in five replicates.

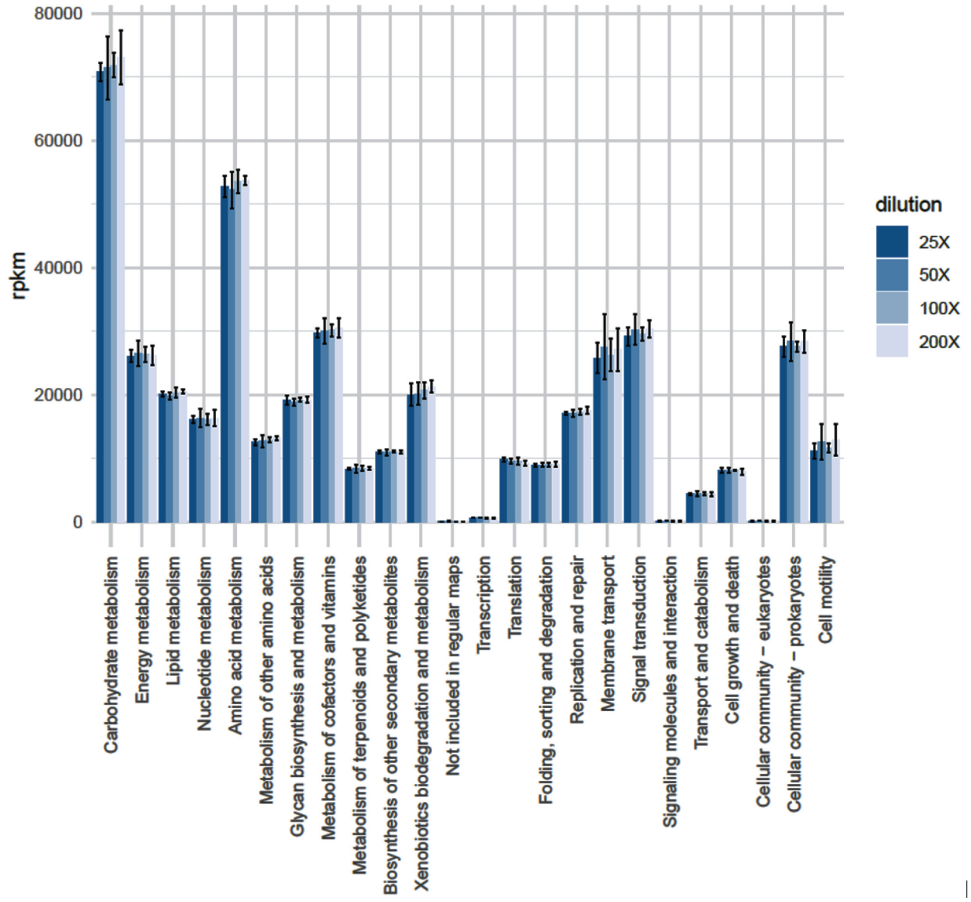

Figure S2. Graph summarising KEGG orthology annotations of rhizosphere metagenomes in four dilutions. The values on y axis are expressed in reads per kilo base per million mapped reads (rpkm). Error bars show the standard deviation of the mean in five replicates.

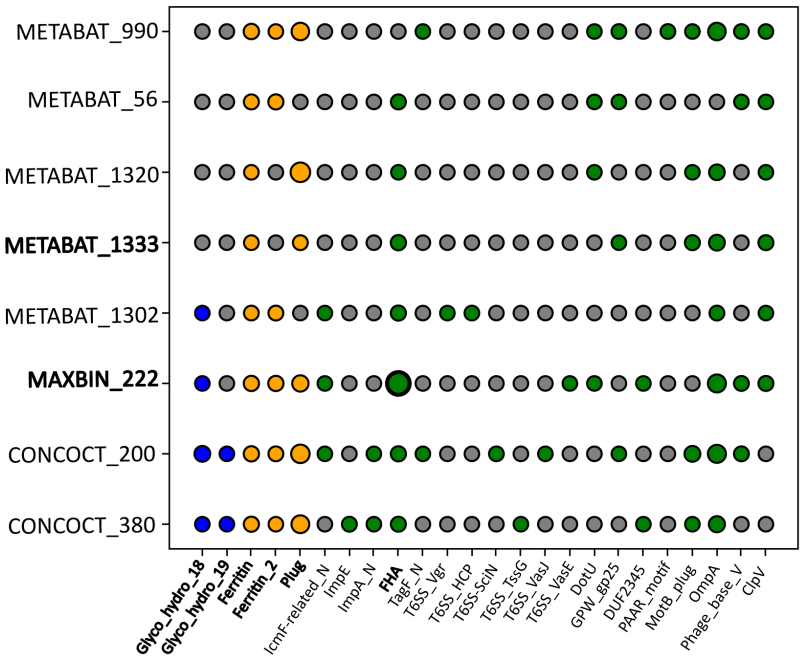

Figure S3. Presence (colored dot) absence (gray dot) patterns of domains contained in KEGG orthologues genes enriched in suppressive dilution points in the MAG collection. Bacterial chitinase families are shown in blue, siderophores associated domains in yellow and components of type VI secretion system in green. ClpV is considered present (last column) if all 4 ClpV subdomains (AAA, AAA_2, AAA_lid_9 and ClpB_D2-small) cooccur on the same contig. FHA domain counts for Labilithrix MAG is shown in bold. Here, multiple core and accessory components of the type VI secretion system are shown.

Table S1. Nonpareil diversity index

	kappa	C	LR	modelR	LRstar	diversity
ESM	0,36975	0,4027322	4,361E+10	0,9994318	1,60E+12	24,86517
25X-1	0,99481	0,9952547	4010631554	0,9965573	2,61E+07	14,62634
25X-2	0,99405	0,9945596	3511713953	0,9967691	2,28E+07	14,45159
25X-3	0,99289	0,9934986	3284871908	0,9971337	1,88E+07	14,38412
25X-4	0,99234	0,9929955	3336073351	0,9970277	1,96E+07	14,36748
25X-5	0,99604	0,9963795	4320103063	0,9966588	2,66E+07	14,65394
50X-1	0,99015	0,9909921	3936582220	0,9968238	2,58E+07	14,57465
50X-2	0,99233	0,9929864	3439318405	0,9969511	2,13E+07	14,39654
50X-3	0,9911	0,9918612	3665552015	0,9967706	2,40E+07	14,50529
50X-4	0,9958	0,99616	3895751514	0,9967257	2,32E+07	14,59096
50X-5	0,99038	0,9912025	3987968934	0,9970652	2,42E+07	14,56012

100X-1	0,99706	0,9973121	2015635523	0,9973075	1,20E+07	13,87775
100X-2	0,99234	0,9929955	2152546737	0,9974004	1,31E+07	13,93182
100X-3	0,99506	0,9954833	2360093190	0,9969755	1,43E+07	14,03799
100X-4	0,99216	0,9928309	1898749915	0,9978125	1,16E+07	13,82418
100X-5	0,99182	0,9925199	2210853791	0,9970134	1,31E+07	14,01849
200X-1	0,99043	0,9912483	2216373822	0,9967982	1,38E+07	13,95889
200X-2	0,99416	0,9946602	1851961914	0,9974601	1,11E+07	13,78291
200X-3	0,99318	0,9937639	2027743164	0,9973221	1,26E+07	13,87862
200X-4	0,99424	0,9947334	1865565389	0,9971779	1,16E+07	13,78712
200X-5	0,99698	0,997239	2092116998	0,9972424	1,35E+07	13,93965

Table S2. Taxonomic groups showing a statistically significant difference between suppressive and conducive phenotype based on deseq2 analysis with adjusted p value (padj) >0.05.

	baseMean	log2FoldChange	lfcSE	stat	pvalue	padj
Phylum						
Chloroflexota_A	39490,725	0,491	0,108	4,533	0,000	0,000
Verrucomicrobiota	1385470,535	0,600	0,138	4,340	0,000	0,000
Nitrospirota	23890,565	0,154	0,036	4,249	0,000	0,000
Bdellovibrionota	222620,736	-0,683	0,162	-4,206	0,000	0,000
Acidobacteriota	368569,397	0,230	0,056	4,134	0,000	0,000
Chloroflexota	112861,105	0,054	0,014	3,913	0,000	0,000
Myxococcota	273855,337	0,304	0,094	3,227	0,001	0,006
Desulfobacterota_A	61305,855	-0,066	0,025	-2,579	0,010	0,034
Firmicutes_C	37613,401	-0,080	0,031	-2,546	0,011	0,034
Planctomycetota	198268,737	0,141	0,056	2,525	0,012	0,034
Proteobacteria	90539661,798	-0,363	0,145	-2,503	0,012	0,034
Gemmatimonadota	112082,072	0,219	0,088	2,487	0,013	0,034
Class						
Alphaproteobacteria	22996742,173	-0,521	0,083	-6,249	0,000	0,000
Vicinamibacteria	111813,239	0,426	0,093	4,564	0,000	0,000
Bacteriovoracia	76844,438	-1,084	0,247	-4,391	0,000	0,000
Acidobacteriae	178419,644	0,092	0,021	4,368	0,000	0,000
Ellin6529	39472,064	0,466	0,108	4,313	0,000	0,000
Verrucomicrobiae	1344083,126	0,594	0,140	4,231	0,000	0,000
Desulfovibrionia	61501,926	-0,088	0,024	-3,616	0,000	0,002
Myxococcia	88014,978	0,246	0,073	3,350	0,001	0,004
Phycisphaerae	48833,733	0,083	0,027	3,125	0,002	0,007
Bdellovibrionia	145735,276	-0,526	0,177	-2,975	0,003	0,010
Blastocatellia	25422,819	0,224	0,076	2,959	0,003	0,010
Polyangia	155993,898	0,332	0,112	2,955	0,003	0,010
Negativicutes	37763,815	-0,102	0,039	-2,641	0,008	0,024
Order						
Acidobacteriales	98538,785	0,115	0,019	6,207	0,000	0,000

Bryobacterales	47288,440	0,194	0,035	5,519	0,000	0,000
Pirellulales	46891,132	0,232	0,044	5,246	0,000	0,000
Rhodospirillales_B	33273,037	-0,160	0,031	-5,185	0,000	0,000
Opitutales	555734,077	1,097	0,220	4,991	0,000	0,000
Nitrospirales	16056,519	0,222	0,045	4,975	0,000	0,000
Sphingomonadales	6161963,173	-0,705	0,143	-4,935	0,000	0,000
Vicinamibacterales	103115,445	0,498	0,103	4,830	0,000	0,000
CSP1-4	34652,118	0,553	0,116	4,779	0,000	0,000
Caulobacterales	4207529,338	-0,572	0,120	-4,767	0,000	0,000
Rhodobacterales	835706,211	-0,171	0,038	-4,504	0,000	0,000
Phycisphaerales	28862,538	0,161	0,038	4,259	0,000	0,000
Rhizobiales	9388973,888	-0,310	0,073	-4,244	0,000	0,000
Rhodospirillales	28924,747	-0,120	0,029	-4,145	0,000	0,000
Myxococcales	88250,073	0,294	0,076	3,853	0,000	0,001
Rhodospirillales_A	38583,001	-0,148	0,039	-3,767	0,000	0,001
Pedosphaerales	136133,148	0,519	0,138	3,758	0,000	0,001
Elusimicrobiales	12380,224	-0,083	0,023	-3,554	0,000	0,002
Micavibrionales	62012,405	-0,579	0,165	-3,506	0,000	0,003
Acidiferrobacterales	11485,584	0,099	0,029	3,453	0,001	0,003
Polyangiales	90226,803	0,506	0,150	3,373	0,001	0,004
Pyrinomonadales	21227,649	0,291	0,089	3,253	0,001	0,006
Haliangiales	14268,707	0,430	0,136	3,164	0,002	0,008
RFP12	12941,743	0,131	0,042	3,118	0,002	0,009
Palsa-1104	20145,003	0,171	0,058	2,954	0,003	0,014
Planctomycetales	23272,475	0,194	0,066	2,928	0,003	0,015
Ferrovibrionales	17106,596	0,422	0,151	2,805	0,005	0,021
Competibacterales	11509,354	-0,093	0,034	-2,745	0,006	0,024
Nevskiales	685807,899	-0,420	0,154	-2,731	0,006	0,025
20CM-4-69-9	12032,020	0,186	0,069	2,711	0,007	0,025
Gemmatimonadales	101811,055	0,246	0,093	2,646	0,008	0,030
Chthoniobacterales	74652,607	0,296	0,113	2,616	0,009	0,031
Bdellovibrionales	145402,464	-0,474	0,185	-2,553	0,011	0,037
Rokubacteriales	69620,443	0,102	0,041	2,480	0,013	0,043
Bacteriovoracales	57229,742	-0,655	0,265	-2,473	0,013	0,043
UBA7541	22119,531	0,097	0,039	2,463	0,014	0,043
Burkholderiales	43343891,188	-0,298	0,122	-2,451	0,014	0,044
Streptomycetales	1466959,322	0,138	0,057	2,422	0,015	0,046
Family						
Koribacteraceae	35374,794	0,165	0,027	6,072	0,000	0,000
Bryobacteraceae	47332,723	0,208	0,039	5,379	0,000	0,000
Nitrospiraceae	14852,896	0,257	0,048	5,395	0,000	0,000
Pirellulaceae	34394,854	0,260	0,050	5,204	0,000	0,000
Opitutaceae	536829,319	1,137	0,226	5,035	0,000	0,000
UBA2999	58261,358	0,563	0,113	4,996	0,000	0,000
Sphingomonadaceae	6160426,173	-0,693	0,144	-4,795	0,000	0,000

Maricaulaceae	23348,656	-0,168	0,035	-4,797	0,000	0,000
CSP1-41	34694,230	0,569	0,118	4,829	0,000	0,000
Magnetospirillaceae	32213,060	-0,153	0,032	-4,732	0,000	0,000
Caulobacteraceae	4104809,357	-0,569	0,124	-4,576	0,000	0,000
SM1A02	21577,933	0,199	0,046	4,311	0,000	0,000
Thalassospiraceae	14696,777	-0,221	0,053	-4,167	0,000	0,000
Rhizobiaceae	4693341,083	-0,536	0,132	-4,071	0,000	0,001
SG8-39	32734,921	0,378	0,095	3,994	0,000	0,001
Pedosphaeraceae	76627,446	0,584	0,147	3,984	0,000	0,001
Myxococcaceae	68699,392	0,346	0,087	3,976	0,000	0,001
Acidobacteriaceae	59741,790	0,104	0,026	3,960	0,000	0,001
Rhodobacteraceae	837358,889	-0,157	0,040	-3,936	0,000	0,001
UBA9959	11274,853	-0,085	0,022	-3,911	0,000	0,001
Akkermansiaceae	133660,860	-0,442	0,120	-3,671	0,000	0,002
AV2	15573,664	0,489	0,139	3,514	0,000	0,004
Polyangiaceae	73382,203	0,558	0,160	3,485	0,000	0,004
GWC2-71-9	42955,815	0,243	0,070	3,479	0,001	0,004
Micavibrionaceae	51138,475	-0,516	0,149	-3,466	0,001	0,004
Rhodospirillaceae	28989,936	-0,106	0,031	-3,413	0,001	0,005
Chitinibacteraceae	23881,359	-0,186	0,055	-3,391	0,001	0,005
Inquilinaceae	13609,211	-0,126	0,038	-3,345	0,001	0,006
Pyrinomonadaceae	21303,299	0,306	0,092	3,322	0,001	0,006
DEV007	19383,070	0,249	0,077	3,252	0,001	0,007
Haliangiaceae	14327,598	0,446	0,137	3,249	0,001	0,007
Demequinaceae	29817,088	0,195	0,060	3,231	0,001	0,008
Phreatobacteraceae	16444,155	-0,265	0,083	-3,194	0,001	0,008
Chitinimonadaceae	11548,946	-0,209	0,066	-3,153	0,002	0,009
Cellulomonadaceae	128381,509	0,223	0,071	3,149	0,002	0,009
UBA10450	41732,871	0,247	0,079	3,149	0,002	0,009
Planctomycetaceae	23343,172	0,209	0,069	3,053	0,002	0,012
Beutenbergiaceae	12593,733	0,185	0,061	3,010	0,003	0,013
Xanthobacteraceae	1526260,733	-0,272	0,092	-2,947	0,003	0,016
Ferrovibrionaceae	17157,291	0,434	0,149	2,915	0,004	0,017
20CM-4-69-91	12069,230	0,202	0,071	2,830	0,005	0,022
Stappiaceae	49373,538	-0,105	0,038	-2,763	0,006	0,027
Nevskiaceae	663860,569	-0,423	0,157	-2,696	0,007	0,032
Ilumatobacteraceae	15569,050	0,335	0,126	2,659	0,008	0,035
UBA1479	9088,574	-0,103	0,039	-2,633	0,008	0,037
UBA75411	21316,019	0,109	0,042	2,614	0,009	0,038
GWA2-73-35	69814,975	0,116	0,045	2,609	0,009	0,038
Streptomycetaceae	1459514,215	0,153	0,060	2,570	0,010	0,041
Bdellovibrionaceae	141832,170	-0,470	0,184	-2,559	0,011	0,042
Fen-1088	14690,777	0,136	0,054	2,515	0,012	0,046
Bacteriovoracaceae	57274,022	-0,643	0,259	-2,488	0,013	0,049

Table S3. Differentially abundant KEGG orthologous (KOs) groups according to bonferroni-corrected exact t-test for occurrence of KOs in differentially abundant contigs versus non differtaially abundant. Only KOs which occurred more often in the first two dilution points are shown here (all oddsratio > 1).

	counts	Total counts	annotation	pvalue	Odds ratio	Bonferroni-corrected pvalue
K01337	167	1216	ko:K01337 E3.4.21.50; lysyl endopeptidase [EC:3.4.21.50]	6,07E-45	3,98	6,95E-41
K21686	192	1563	ko:K21686 prpR; XRE family transcriptional regulator, fatty acid utilization regulator	3,21E-44	3,50	3,68E-40
K03088	2206	42449	ko:K03088 rpoE; RNA polymerase sigma-70 factor, ECF subfamily	5,13E-43	1,37	5,88E-39
K12132	676	10515	ko:K12132 prkC, stkP; eukaryotic-like serine/threonine-protein kinase [EC:2.7.11.1]	1,48E-36	1,72	1,69E-32
K07713	144	1261	ko:K07713 zraR, hydG; two-component system, NtrC family, response regulator HydG	2,85E-30	3,22	3,27E-26
K02456	282	3593	ko:K02456 gspG; general secretion pathway protein G	2,94E-28	2,13	3,37E-24
K03407	236	2818	ko:K03407 cheA; two-component system, chemotaxis family, sensor kinase CheA [EC:2.7.13.3]	1,09E-27	2,29	1,25E-23
K05499	190	2063	ko:K05499 cytR; LacI family transcriptional regulator, repressor for deo operon, udp, cdd, tsx, nupC, and nupG	2,22E-27	2,54	2,54E-23
K03932	217	2788	ko:K03932 lpqC; polyhydroxybutyrate depolymerase	9,71E-22	2,11	1,11E-17
K07114	516	8716	ko:K07114 yfbK; Ca-activated chloride channel homolog	5,34E-21	1,57	6,12E-17
K03559	248	3543	ko:K03559 exbD; biopolymer transport protein ExbD	9,60E-19	1,88	1,10E-14
K03301	83	746	ko:K03301 TC.AAA; ATP:ADP antiporter, AAA family	1,63E-17	3,13	1,87E-13
K03561	154	1938	ko:K03561 exbB; biopolymer transport protein ExbB	1,07E-16	2,16	1,22E-12
K20444	439	7595	ko:K20444 rfbC; O-antigen biosynthesis protein [EC:2.4.1.-]	1,77E-16	1,53	2,03E-12
K02669	174	2316	ko:K02669 pilT; twitching motility protein PilT	2,33E-16	2,03	2,67E-12
K10941	67	555	ko:K10941 fleQ, flrA; sigma-54 dependent transcriptional regulator, flagellar regulatory protein	3,42E-16	3,43	3,92E-12

K02078	226	3386	ko:K02078 acpP; acyl carrier protein	4,66E-15	1,79	5,34E-11
K04767	34	181	ko:K04767 acuB; acetoin utilization protein AcuB	2,09E-14	5,78	2,39E-10
K07011	308	5097	ko:K14652 ribBA; 3,4-dihydroxy 2-butanone 4-phosphate synthase / GTP cyclohydrolase II [EC:4.1.99.12 3.5.4.25]	2,69E-14	1,61	3,09E-10
K02065	188	2804	ko:K02065 mlaF, linL, mkl; phospholipid/cholesterol/gamma-HCH transport system ATP-binding protein	5,56E-13	1,80	6,37E-09
K20276	961	19857	ko:K20276 bapA; large repetitive protein	1,44E-12	1,27	1,65E-08
K03973	116	1494	ko:K03973 pspC; phage shock protein C	2,35E-12	2,10	2,69E-08
K07315	238	3872	ko:K07315 rsbU_P; phosphoserine phosphatase RsbU/P [EC:3.1.3.3]	3,94E-12	1,64	4,51E-08
K12982	57	525	ko:K12982 opsX; heptosyltransferase I [EC:2.4.-.-]	4,12E-12	3,04	4,72E-08
K03972	40	290	ko:K03972 pspE; phage shock protein E	4,20E-12	4,00	4,81E-08
K09697	128	1731	ko:K09697 natA; sodium transport system ATP-binding protein [EC:7.2.2.4]	5,04E-12	2,00	5,77E-08
K03594	265	4439	ko:K03594 bfr; bacterioferritin [EC:1.16.3.1]	5,28E-12	1,59	6,05E-08
K09691	172	2576	ko:K09691 ABC-2.LPSE.A; lipopolysaccharide transport system ATP-binding protein	7,03E-12	1,79	8,06E-08
K07322	63	624	ko:K07322 ytfE, scdA; regulator of cell morphogenesis and NO signaling	7,59E-12	2,81	8,70E-08
K06076	147	2104	ko:K06076 fadL; long-chain fatty acid transport protein	9,42E-12	1,88	1,08E-07
K12287	222	3603	ko:K12287 mshQ; MSHA biogenesis protein MshQ	1,60E-11	1,64	1,83E-07
K03413	263	4451	ko:K03413 cheY; two-component system, chemotaxis family, chemotaxis protein CheY	1,75E-11	1,57	2,01E-07
K02662	105	1351	ko:K02662 pilM; type IV pilus assembly protein PilM	2,30E-11	2,11	2,64E-07
K03744	176	2715	ko:K03744 lemA; LemA protein	4,14E-11	1,73	4,74E-07
K07714	99	1263	ko:K07714 atoC; two-component system, NtrC family, response regulator AtoC	5,22E-11	2,13	5,98E-07
K03768	280	4860	ko:K03768 PPIB, ppiB; peptidyl-prolyl cis-trans isomerase B (cyclophilin B) [EC:5.2.1.8]	5,37E-11	1,53	6,16E-07
K11894	27	160	ko:K11894 impI, vasC; type VI secretion system protein ImpI	1,22E-10	5,08	1,39E-06
K02003	416	7853	ko:K02003 ABC.CD.A; putative ABC transport system ATP-binding protein	1,36E-10	1,40	1,55E-06

K03924	357	6562	ko:K03924 moxR; MoxR-like ATPase [EC:3.6.3.-]	1,39E-10	1,44	1,59E-06
K01990	627	12607	ko:K01990 ABC-2.A; ABC-2 type transport system ATP-binding protein	1,64E-10	1,31	1,88E-06
K08084	119	1661	ko:K08084 fimT; type IV fimbrial biogenesis protein FimT	1,83E-10	1,93	2,09E-06
K09928	78	937	ko:K09928 K09928; uncharacterized protein	3,60E-10	2,27	4,13E-06
K03640	164	2555	ko:K03640 pal; peptidoglycan-associated lipoprotein	3,68E-10	1,71	4,22E-06
K03671	262	4607	ko:K03671 trxA; thioredoxin 1	7,06E-10	1,51	8,09E-06
K00702	23	129	ko:K00702 E2.4.1.20; cellobiose phosphorylase [EC:2.4.1.20]	9,10E-10	5,42	1,04E-05
K15876	26	163	ko:K15876 nrfH; cytochrome c nitrite reductase small subunit	9,36E-10	4,74	1,07E-05
K09696	67	780	ko:K09696 natB; sodium transport system permease protein	1,69E-09	2,35	1,93E-05
K02911	75	918	ko:K02911 RP-L32, MRPL32, rpmF; large subunit ribosomal protein L32	1,73E-09	2,22	1,99E-05
K02851	110	1557	ko:K02851 wecA, tagO, rfe; UDP-GlcNAc:undecaprenyl-phosphate/decaprenyl-phosphate GlcNAc-1-phosphate transferase [EC:2.7.8.33 2.7.8.35]	1,83E-09	1,90	2,09E-05
K06180	228	3940	ko:K06180 rluD; 23S rRNA pseudouridine1911/1915/1917 synthase [EC:5.4.99.23]	2,03E-09	1,54	2,33E-05
K09992	272	4887	ko:K09992 K09992; uncharacterized protein	2,50E-09	1,47	2,87E-05
K03086	197	3303	ko:K03086 rpoD; RNA polymerase primary sigma factor	2,55E-09	1,59	2,92E-05
K13668	60	673	ko:K13668 pimB; phosphatidyl-myo-inositol dimannoside synthase [EC:2.4.1.346]	2,91E-09	2,45	3,34E-05
K02477	213	3643	ko:K02477 K02477; two-component system, LytTR family, response regulator	2,96E-09	1,55	3,40E-05
K03564	216	3711	ko:K03564 BCP, PRXQ, DOT5; thioredoxin-dependent peroxiredoxin [EC:1.11.1.24]	3,31E-09	1,55	3,79E-05
K00368	129	1941	ko:K00368 nirK; nitrite reductase (NO-forming) [EC:1.7.2.1]	3,35E-09	1,78	3,84E-05
K01992	750	15731	ko:K01992 ABC-2.P; ABC-2 type transport system permease protein	3,75E-09	1,25	4,30E-05
K02916	64	747	ko:K02916 RP-L35, MRPL35, rpmI; large subunit ribosomal protein L35	4,21E-09	2,34	4,83E-05
K08976	96	1319	ko:K08976 K08976; putative membrane protein	4,38E-09	1,96	5,01E-05

K09690	122	1817	ko:K09690 ABC-2.LPSE.P; lipopolysaccharide transport system permease protein	4,89E-09	1,80	5,60E-05
K10914	344	6519	ko:K10914 crp; CRP/FNR family transcriptional regulator, cyclic AMP receptor protein	7,02E-09	1,39	8,04E-05
K07031	52	562	ko:K07031 hddA; D-glycero-alpha-D-manno-heptose-7-phosphate kinase [EC:2.7.1.168]	9,23E-09	2,55	1,06E-04
K20333	20	112	ko:K20333 toxD; toxoflavin biosynthesis protein ToxD	1,07E-08	5,43	1,23E-04
K03560	181	3040	ko:K03560 tolR; biopolymer transport protein TolR	1,21E-08	1,58	1,39E-04
K07027	127	1946	ko:K07027 K07027; glycosyltransferase 2 family protein	1,24E-08	1,75	1,42E-04
K03562	235	4183	ko:K03562 tolQ; biopolymer transport protein TolQ	1,34E-08	1,49	1,53E-04
K19302	373	7209	ko:K19302 bcrC; undecaprenyl-diphosphatase [EC:3.6.1.27]	1,38E-08	1,36	1,58E-04
K02282	300	5614	ko:K02282 cpaE, tadZ; pilus assembly protein CpaE	1,93E-08	1,41	2,22E-04
K02650	137	2164	ko:K02650 pilA; type IV pilus assembly protein PilA	2,10E-08	1,69	2,41E-04
K10909	31	255	ko:K10909 luxQ; two-component system, autoinducer 2 sensor kinase/phosphatase LuxQ [EC:2.7.13.3 3.1.3.-]	2,11E-08	3,46	2,41E-04
K01399	6	7	ko:K01399 lasB; pseudolysin [EC:3.4.24.26]	2,19E-08	150,00	2,51E-04
K19411	43	433	ko:K19411 mcsA; protein arginine kinase activator	2,25E-08	2,76	2,58E-04
K05808	92	1290	ko:K05808 yhbH; putative sigma-54 modulation protein	2,31E-08	1,92	2,64E-04
K02655	117	1772	ko:K02655 pilE; type IV pilus assembly protein PilE	2,41E-08	1,77	2,76E-04
K03935	18	96	ko:K03935 NDUFS2; NADH dehydrogenase (ubiquinone) Fe-S protein 2 [EC:7.1.1.2]	2,60E-08	5,77	2,98E-04
K03183	185	3159	ko:K03183 ubiE; demethylmenaquinone methyltransferase / 2-methoxy-6-polyprenyl-1,4-benzoquinol methylase [EC:2.1.1.163 2.1.1.201]	2,67E-08	1,56	3,07E-04
K03272	92	1299	ko:K03272 gmhC, hldE, waaE, rfaE; D-beta-D-heptose 7-phosphate kinase / D-beta-D-heptose 1-phosphate adenosyltransferase [EC:2.7.1.167 2.7.7.70]	3,17E-08	1,91	3,63E-04

K20628	48	522	ko:K20628 exlX; expansin	4,01E-08	2,53	4,59E-04
K02485	45	476	ko:K02485 rssB, hnr; two-component system, response regulator	4,65E-08	2,61	5,33E-04
K03624	126	1974	ko:K03624 greA; transcription elongation factor GreA	4,77E-08	1,70	5,47E-04
K20534	132	2095	ko:K20534 gtrB, csbB; polyisoprenyl-phosphate glycosyltransferase [EC:2.4.-.-]	4,87E-08	1,68	5,58E-04
K00428	165	2772	ko:K00428 E1.11.1.5; cytochrome c peroxidase [EC:1.11.1.5]	5,16E-08	1,58	5,91E-04
K16291	62	765	ko:K16291 erfK; L,D-transpeptidase ErfK/SrfK	5,45E-08	2,20	6,24E-04
K20543	136	2189	ko:K20543 bcsC; cellulose synthase operon protein C	6,87E-08	1,66	7,87E-04
K02887	74	990	ko:K02887 RP-L20, MRPL20, rplT; large subunit ribosomal protein L20	8,29E-08	2,02	9,50E-04
K02437	120	1876	ko:K02437 gcvH, GCSH; glycine cleavage system H protein	8,68E-08	1,71	9,95E-04
K04749	73	975	ko:K04749 rsbV; anti-sigma B factor antagonist	9,45E-08	2,02	1,08E-03
K03179	96	1408	ko:K03179 ubiA; 4-hydroxybenzoate polyprenyltransferase [EC:2.5.1.39]	9,52E-08	1,83	1,09E-03
K01218	155	2593	ko:K01218 gmuG; mannan endo-1,4-beta-mannosidase [EC:3.2.1.78]	9,83E-08	1,59	1,13E-03
K15518	33	303	ko:K15518 dgk; deoxyguanosine kinase [EC:2.7.1.113]	1,08E-07	3,06	1,24E-03
K03060	76	1037	ko:K03060 rpoZ; DNA-directed RNA polymerase subunit omega [EC:2.7.7.6]	1,23E-07	1,98	1,41E-03
K22489	15	74	ko:K22489 hosA; MarR family transcriptional regulator, temperature-dependent positive regulator of motility	1,26E-07	6,36	1,44E-03
K07814	120	1896	ko:K07814 K07814; putative two-component system response regulator	1,50E-07	1,69	1,72E-03
K22391	112	1737	ko:K22391 E3.5.4.16; GTP cyclohydrolase I [EC:3.5.4.16]	1,53E-07	1,72	1,75E-03
K00809	59	736	ko:K00809 DHPS, dys; deoxyhypusine synthase [EC:2.5.1.46]	1,61E-07	2,18	1,85E-03
K00940	97	1445	ko:K00940 ndk, NME; nucleoside-diphosphate kinase [EC:2.7.4.6]	1,66E-07	1,80	1,91E-03
K19668	77	1065	ko:K19668 CBH2, cbhA; cellulose 1,4-beta-cellobiosidase [EC:3.2.1.91]	1,74E-07	1,95	2,00E-03
K13628	63	810	ko:K13628 iscA; iron-sulfur cluster assembly protein	1,84E-07	2,11	2,10E-03
K12506	103	1566	ko:K12506 ispDF; 2-C-methyl-D-erythritol 4-phosphate cytidylyltransferase / 2-C-methyl-D-erythritol 2,4-cyclodiphosphate synthase [EC:2.7.7.60 4.6.1.12]	1,86E-07	1,76	2,14E-03

K02663	67	884	ko:K02663 pilN; type IV pilus assembly protein PilN	1,98E-07	2,05	2,27E-03
K06377	18	110	ko:K06377 spo0M; sporulation-control protein	2,27E-07	4,89	2,60E-03
K06881	59	751	ko:K06881 nrnA; bifunctional oligoribonuclease and PAP phosphatase NrnA [EC:3.1.3.7 3.1.13.3]	3,15E-07	2,13	3,61E-03
K02666	122	1966	ko:K02666 pilQ; type IV pilus assembly protein PilQ	3,26E-07	1,65	3,74E-03
K03271	62	806	ko:K03271 gmhA, lpcA; D-sedoheptulose 7-phosphate isomerase [EC:5.3.1.28]	3,32E-07	2,08	3,80E-03
K07003	242	4518	ko:K07003 K07003; uncharacterized protein	3,41E-07	1,41	3,91E-03
K03530	113	1788	ko:K03530 hupB; DNA-binding protein HU-beta	3,59E-07	1,69	4,11E-03
K03832	506	10514	ko:K03832 tonB; periplasmic protein TonB	3,81E-07	1,26	4,37E-03
K06142	120	1935	ko:K06142 hlpA, ompH; outer membrane protein	4,16E-07	1,65	4,77E-03
K12984	91	1360	ko:K12984 waaE, kdtX; (heptosyl)LPS beta-1,4-glucosyltransferase [EC:2.4.1.-]	4,45E-07	1,79	5,10E-03
K18285	63	835	ko:K18285 mqnE; aminodeoxyfutalosine synthase [EC:2.5.1.120]	5,19E-07	2,04	5,95E-03
K01179	488	10130	ko:K01179 E3.2.1.4; endoglucanase [EC:3.2.1.4]	5,41E-07	1,27	6,20E-03
K08481	58	747	ko:K08481 kaiB; circadian clock protein KaiB	5,74E-07	2,10	6,58E-03
K02914	52	641	ko:K02914 RP-L34, MRPL34, rpmH; large subunit ribosomal protein L34	5,84E-07	2,21	6,69E-03
K21147	156	2697	ko:K21147 moeZR, moeBR; sulfur-carrier protein adenylyltransferase/sulfurtransferase [EC:2.7.7.80 2.7.7.- 2.8.1.11 2.8.1.-]	6,13E-07	1,53	7,02E-03
K05337	96	1475	ko:K05337 fer; ferredoxin	7,38E-07	1,74	8,45E-03
K20074	241	4547	ko:K20074 prpC, phpP; PPM family protein phosphatase [EC:3.1.3.16]	7,73E-07	1,40	8,85E-03
K02237	134	2249	ko:K02237 comEA; competence protein ComEA	7,95E-07	1,58	9,12E-03
K02356	105	1657	ko:K02356 efp; elongation factor P	7,96E-07	1,69	9,13E-03
K10947	88	1323	ko:K10947 padR; PadR family transcriptional regulator, regulatory protein PadR	8,62E-07	1,78	9,88E-03
K12686	80	1169	ko:K12686 apeE, estA, lip-1; outer membrane lipase/esterase	8,93E-07	1,84	1,02E-02
K02612	126	2090	ko:K02612 paaD; ring-1,2-phenylacetyl-CoA epoxidase subunit PaaD	9,22E-07	1,60	1,06E-02

K01512	76	1096	ko:K01512 acyP; acylphosphatase [EC:3.6.1.7]	1,01E-06	1,86	1,16E-02
K13658	19	134	ko:K13658 gumI; beta-1,4-mannosyltransferase [EC:2.4.1.251]	1,04E-06	4,13	1,19E-02
K02110	73	1041	ko:K02110 ATPF0C, atpE; F-type H+-transporting ATPase subunit c	1,08E-06	1,89	1,24E-02
K01953	245	4661	ko:K01953 asnB, ASNS; asparagine synthase (glutamine-hydrolysing) [EC:6.3.5.4]	1,15E-06	1,39	1,32E-02
K01183	155	2710	ko:K01183 E3.2.1.14; chitinase [EC:3.2.1.14]	1,24E-06	1,52	1,42E-02
K08998	142	2437	ko:K08998 K08998; uncharacterized protein	1,27E-06	1,55	1,46E-02
K19342	35	370	ko:K19342 nosL; copper chaperone NosL	1,32E-06	2,61	1,51E-02
K02884	79	1166	ko:K02884 RP-L19, MRPL19, rplS; large subunit ribosomal protein L19	1,51E-06	1,82	1,73E-02
K07778	50	628	ko:K07778 desK; two-component system, NarL family, sensor histidine kinase DesK [EC:2.7.13.3]	1,61E-06	2,16	1,85E-02
K09121	39	439	ko:K09121 larC; pyridinium-3,5-bisthiocarboxylic acid mononucleotide nickel chelatase [EC:4.99.1.12]	1,63E-06	2,44	1,86E-02
K13573	41	473	ko:K13573 pafC; proteasome accessory factor C	1,67E-06	2,37	1,91E-02
K02847	74	1073	ko:K02847 waaL, rfaL; O-antigen ligase [EC:2.4.1.-]	1,68E-06	1,85	1,93E-02
K02653	198	3652	ko:K02653 pilC; type IV pilus assembly protein PilC	1,70E-06	1,43	1,95E-02
K02909	77	1133	ko:K02909 RP-L31, rpmE; large subunit ribosomal protein L31	1,81E-06	1,82	2,08E-02
K07107	291	5737	ko:K07107 ybgC; acyl-CoA thioester hydrolase [EC:3.1.2.-]	2,24E-06	1,34	2,57E-02
K04078	92	1437	ko:K04078 groES, HSPE1; chaperonin GroES	2,39E-06	1,71	2,74E-02
K02066	238	4558	ko:K02066 mlaE, linK; phospholipid/cholesterol/gamma-HCH transport system permease protein	2,54E-06	1,38	2,91E-02
K12340	198	3678	ko:K12340 tolC; outer membrane protein	2,64E-06	1,42	3,03E-02
K18431	54	712	ko:K18431 legF, ptmB; CMP-N,N'-diacetyllegionaminic acid synthase [EC:2.7.7.82]	2,73E-06	2,05	3,12E-02
K20468	26	243	ko:K20468 K20468; putative heme transporter	3,14E-06	3,00	3,60E-02
K03298	41	486	ko:K03298 TC.DME; drug/metabolite transporter, DME family	3,27E-06	2,30	3,75E-02

K07220	92	1449	ko:K07220 K07220; uncharacterized protein	3,33E-06	1,69	3,82E-02
K03116	63	890	ko:K03116 tatA; sec-independent protein translocase protein TatA	4,15E-06	1,90	4,75E-02
K05988	34	373	ko:K05988 dexA; dextranase [EC:3.2.1.11]	4,16E-06	2,51	4,77E-02
K22205	49	632	ko:K22205 K22205; S-adenosyl-L-methionine hydrolase (adenosine-forming) [EC:3.13.1.8]	4,21E-06	2,10	4,82E-02
K04760	66	948	ko:K04760 greB; transcription elongation factor GreB	4,30E-06	1,87	4,93E-02

Table S4. AntiSMASH-predicted occurrences of biosynthetic gene clusters (separated by gene cluster product class according to antiSMASH output) in differentially abundant contigs (more abundant in the suppressive dilutions 25X and 50X) versus the rest of the assembly. Statistical results are based on Fisher exact test, significant results are highlighted in bold.

BGC product	Counts on DE contigs	Counts on NOT DE contigs	ODDS Ratio	P-value
arylpolyene	65	373	1,5145	0,0056
melanin	2	2	inf	0,0150
acyl amino acids	10	157	0,4882	0,0240
ladderane	6	20	3,0757	0,0289
T3PKS	43	260	1,4221	0,0523
NRPS-like	44	278	1,3494	0,0905
betalactone	16	86	1,6404	0,0950
NRPS	69	690	0,7974	0,0988
other	4	15	2,6097	0,1021
T1PKS	18	213	0,6625	0,1055
T2PKS	1	1	inf	0,1225
NAGGN	0	18	0,0000	0,1546
resorcinol	11	59	1,6446	0,1586
proteusin	1	2	7,1766	0,2300
lanthipeptide	4	60	0,5126	0,2343
hglE-KS	7	40	1,5223	0,3282
TfuA-related	3	46	0,5007	0,3610
linaridin	0	11	0,0000	0,3802
phosphonate	6	37	1,3890	0,4478
lassopeptide	15	150	0,7974	0,5238

LAP	2	29	0,5316	0,5699
hserlactone	21	196	0,8612	0,5775
transAT-PKS	0	8	0,0000	0,6070
ectoine	3	38	0,6151	0,6170
butyrolactone	2	14	1,1961	0,6859
bacteriocin	62	486	1,0494	0,7153
indole	3	32	0,7424	0,7907
siderophore	10	89	0,9084	0,8712
terpene	73	605	0,9848	0,9471
CDPS	0	5	0,0000	1,0000
PKS-like	0	7	0,0000	1,0000
transAT-PKS-like	3	30	0,7974	1,0000
amglyccycl	0	4	0,0000	1,0000
microviridin	0	6	0,0000	1,0000
furan	0	2	0,0000	1,0000
thiopeptide	0	5	0,0000	1,0000
cyanobactin	0	3	0,0000	1,0000
phenazine	0	2	0,0000	1,0000
nucleoside	0	1	0,0000	1,0000
oligosaccharide	0	1	0,0000	1,0000
PpyS-KS	0	2	0,0000	1,0000